Crystallization of (012) oriented calcite single crystals underneath monolayers of tetra(carboxymethoxy)calix[4]arenes †

Dirk Volkmer,*[a] Marc Fricke,[a] Dieter Vollhardt[b] and Stefan Siegel[b]

[a] *Faculty of Chemistry (AC1), University of Bielefeld, P.O. Box 100 131, D-33501 Bielefeld, Germany. E-mail: dirk.volkmer@uni-bielefeld.de*
[b] *Max-Planck-Institute of Colloids and Interfaces, MPI-KG Golm, D-14424 Potsdam, Germany. E-mail: dieter.vollhardt@mpikg-golm.mpg.de*

The amphiphilic 5,11,17,23-tetrakis(1,1,3,3-tetramethylbutyl)-25,26,27,28-tetra(carboxymethoxy)calix[4]arene, **1**, forms stable monolayers at the air–water interface which can be employed as supramolecular templates for induced calcite crystallization. Uniform, (012) oriented $CaCO_3$ (calcite) single crystals grow underneath monolayers of **1** at low compression (π = 0.1–0.5 mN m^{-1}), while more randomly oriented single crystals are obtained at higher surface pressure (π = 5–20 mN m^{-1}). The use of easy-to-synthesize calixarenes for this particular area of crystal engineering is reported here for the first time. A range of structural analysis methods is employed in order to obtain a refined picture of the structural factors that govern the growth of uniformly oriented calcite crystals underneath monolayers of **1**. Thus, the crystal structures of 5,11,17,23-tetrakis(1,1,3,3-tetramethylbutyl)-25,26,27,28-tetra(carboxymethoxy)-calix[4]arene, **1**, as well as of its Ca salt, **2**, were solved and analysed in terms of typical supramolecular packing arrangements and coordination motifs. The Langmuir isotherms point to a liquid-condensed state of the monolayers of **1** throughout the investigated compression range. Brewster angle microscopic observation of the monolayer morphology at low surface pressure reveals a highly viscous consistency, which does not change upon further compression. Grazing incidence X-ray diffraction (GIXD) investigations on the monolayer structure provide no indications for the occurrence of a two-dimensional lattice of the alkyl chains. Considering the non-crystalline, highly dynamic state of the monolayer during crystal maturation, an epitaxial correlation based on geometric matching of lattice positions between the monolayer and the overgrowing calcite crystals is ruled out. We, therefore, suggest that non-specific monolayer properties such as average charge density or mean dipole moment are the main determinants for templated calcite growth in the present and related cases.

Introduction

Much attention has been devoted to the characterization of mineral phases which occur in biominerals and calcified tissues.[1] Apart from aesthetically pleasant, intricate shapes, biominerals often possess attractive materials properties that attribute to a sophisticated internal hierarchical structure.[2] Among the many open questions, one of the most challenging scientific goals is to gain insights into the molecular interactions that occur at the interface between the inorganic mineral and the macromolecular organic matrix.

For the most widespread calcified tissues it is frequently assumed that a structurally rigid composite matrix consisting of fibrous proteins and thereon adsorbed acidic macromolecules acts as a supramolecular "blueprint" that templates nucleation of the inorganic phase.[3]

Efforts aimed at trying to mimic aspects of these complex interactions with simple model systems will help to improve our understanding of crystallization processes that are under biological control. However, the deliberate design of interface architectures that direct the crystal nucleation and growth of inorganic crystal phases in a predictable manner is by and large still a matter of trial and error. Chemists have employed different experimental set-ups to create highly-ordered template surfaces, including Langmuir monolayers,[4] or self-assembled monolayers (SAMs).[5] In particular, the crystallization of inorganic compounds underneath free floating monolayers of amphiphilic molecules bears much development potential, since the surface properties may be adjusted by a suitable surfactant design as well as by simple experimental parameters (*i.e.* subphase composition, surface area per molecule, or temperature).

We have initiated a research project which focuses on induced $CaCO_3$ crystallization underneath Langmuir monolayers of amphiphilic oligoacids. The envisaged molecular library (Scheme 1) consists of macrocyclic oligo(2-carboxymethoxy-5-(alkyl)-1,3-phenyl)methylene derivatives (I) ("calix[*n*]arenes") and their open-chain derivatives (II).

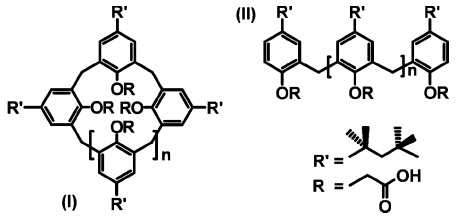

Scheme 1

Employing macrocyclic amphiphiles we would like to address the rather fundamental question concerning the putative structure of crystal nucleation sites in calcified tissues. Investigations on the amino acid composition of different natural proteins associated with biomineralisation reveal sequence motifs which are particularly rich in aspartic and glutamic acid residues, respectively.[6] Unfortunately, none of the acidic proteins extracted from calcified tissues have yet been grown into single crystals suitable for X-ray crystallographic investigations and thus three-dimensional structures are currently

† Electronic supplementary information (ESI) available: synthesis and characterization details and atom numbering schemes for **1** and **2**. See http://www.rsc.org/suppdata/dt/b2/b206912a/

not available. However, a representative structural model of a mineral/peptide interface architecture may be derived from the iron storage protein (ferritin) which is regarded as an archetypal biological model for the formation of a nanocrystalline mineral phase within a confined space.[7] Here, the ferritin L-chain subunit bears four suitably aligned glutamic acid residues that are necessary for mineral formation. Artificial organic molecules can be designed so as to mimic the confined arrangement of acidic residues in natural proteins. Macrocyclic calix[*n*]arenes such as (I) are especially suited for this purpose since they are synthetically readily available. These molecules form confined arrays of co-aligned carboxylic acid groups, the number and relative positions of which show systematic structural variations depending on the size of the macrocyclic backbone. Previous studies on calcium carbonate crystallization underneath surfactant monolayers have not addressed the particular question of whether or not *single template molecules* can induce crystal nucleation. However, related investigations have been reported recently, focussing on the *minimum size of segregated hydroxyl domains* in mixed Langmuir films for inducing ice nucleation.[8]

Here we present the first results on induced crystallization of calcium carbonate underneath monolayers of one member of the molecular library of amphiphilic oligoacids (Scheme 1), namely 5,11,17,23-tetrakis(1,1,3,3-tetramethylbutyl)-25,26,27,-28-tetra(carboxymethoxy)calix[4]arene, **1**. The crystal structures of the free acid and its Ca salt **2** are investigated by means of single crystal X-ray crystallography. Monolayers of **1** are spread on aqueous subphases and the resulting isotherms are analysed in terms of possible supramolecular packing arrangements. The dynamic macroscopic monolayer structure is characterized by means of Brewster angle microscopy (BAM) and grazing incidence X-ray diffraction (GIXD). The growth of uniformly (012) oriented calcite ($CaCO_3$) single crystals underneath monolayers of **1** is monitored *in situ* by (polarization) optical microscopy. The orientation of calcite crystals relative to the monolayer is determined by means of X-ray diffraction, scanning electron microscopy and optical microscopy.

Results and discussion

NMR spectroscopy

The ^{1}H-NMR spectra of **1** in $CDCl_3$ solution show the characteristic doublet splitting of the CH_2 resonance signal (δ = 4.59 and 3.25, ^2J = 7.1 Hz) of the macrocyclic methylene protons, which shows that there is no interconversion between the main four calix[4]arene conformers.[9] The 1,1,3,3-tetramethylbutyl resonance signals (and the carboxymethoxy substituents, respectively) on the other hand display sharp singlet signals indicating a high rotational flexibility of the pendant calixarene substituents.

The ^{1}H- and ^{13}C-NMR spectra of **2** in $CDCl_3$ solution show characteristic chemical shifts which are indicative of metal complex formation.[10] In the ^{1}H-NMR spectrum of **2**, the aromatic protons display a downfield shift as compared to the resonance signal of the non-coordinated calixarene ligand **1**. The separation of the CH_2 resonance signal (δ = 4.27 and 3.35, ^2J = 12.3 Hz) of the macrocyclic methylene protons decreases while the CH_2 resonance signal of the carboxymethoxy substituents splits into a doublet of doublets (δ = 5.10 and 3.96, ^2J = 14.3 Hz).

X-Ray crystallographic investigations

Structural analyses of calixarenes comprising the sterically demanding 1,1,3,3-tetramethylbutyl group are rare. A search of the Cambridge structural database (October 2002) yielded a total of four X-ray structures.[11] The X-ray crystallographic investigations on single crystals of 5,11,17,23-tetrakis(1,1,3,3-tetramethylbutyl)-25,26,27,28-tetra(carboxymethoxy)calix[4]-arene and its Ca salt presented here are the first examples of a metal-free calix[*n*]arene acid and its corresponding Ca complex.

Crystal structure of 1. Single crystals of the compound $C_{68}H_{96}O_{12}\cdot 4.75CH_3OH\cdot 0.25H_2O$ (**1**) were obtained from a methanol solution containing 10% of water. The X-ray structure analysis shows that the calix[4]arene molecules adapt a highly symmetrical cone-conformation where the hydrophobic *para*-substituents are placed at stereochemically equivalent positions (Fig. 1a). Due to crystal packing effects the

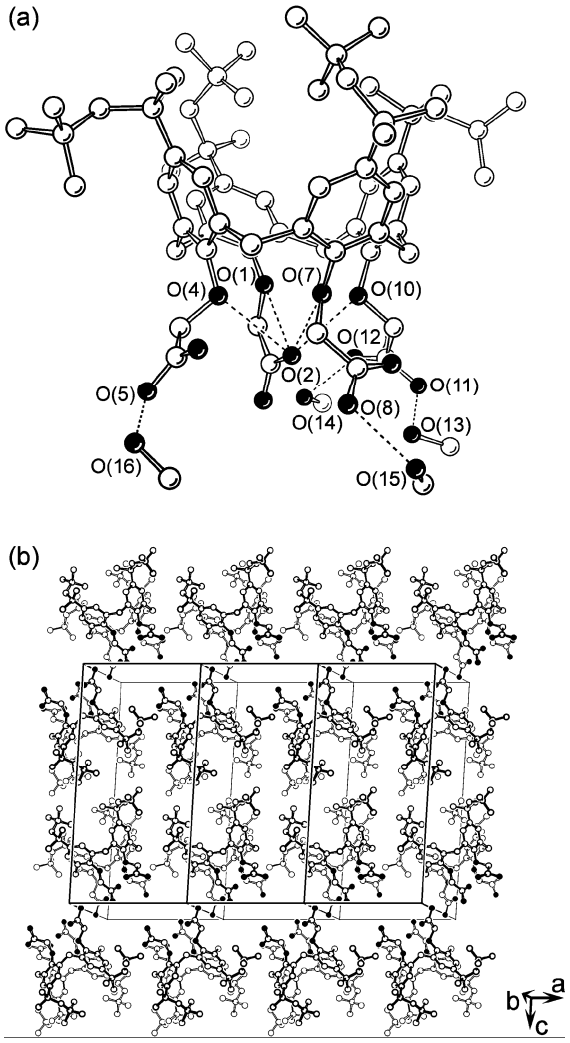

Fig. 1 (a) Ball-and-stick model of the molecular structure of **1** (hydrogen atoms are omitted for clarity). The atomic numbering scheme indicates those oxygen pairs which form strong hydrogen bonds. Non-bonding (intramolecular) oxygen–oxygen distances: O(2) ··· O(1) 2.638(1), O(2) ··· O(4) 3.060(2), O(2) ··· O(7) 2.811(2), O(2) ··· O(10) 2.845(1) Å. Closest (intermolecular) oxygen–oxygen distances between carboxylic acid groups and crystal methanol molecules: O(5) ··· O(16) 2.622(1), O(8) ··· O(15) 2.589(1), O(11) ··· O(13) 2.553(2), O(12) ··· O(14) 2.767(1) Å. (b) Ball-and-stick model of the supramolecular packing arrangement of **1** in the crystal lattice (methanol molecules and hydrogen atoms are omitted for clarity).

calixarene moiety differs significantly from idealized C_{4v} point symmetry. First, the 1,1,3,3-tetramethylbutyl groups become irregularly placed such that two of them point inside the calixarene cavity, while the neighbouring hydrophobic residues are bent outwards. As a consequence, no further molecular guests are located within the internal cavities of **1** or **2**, in contrast to host–guest inclusion phenomena frequently observed in conjunction with structurally similar *tert*-butylcalix[4]arene hosts.[12] This structural behaviour seems rather typical for

calix[4]arene molecules containing the sterically demanding 1,1,3,3-tetramethylbutyl substituent, since similar arrangements are found in the crystal structures of 5,11,17,23-tetrakis(1,1,3,3-tetramethylbutyl)-25,26,27,28-tetrahydroxycalix(4)arene,[13] and of *exo-endo*-25,26,27,28-bis(n-butoxyphosphoryl)-5,11,17,23-tetrakis(1,1,3,3-tetramethylbutyl)calix(4)arene, respectively.[14]

As a second distinctive feature, the molecular structure of **1** shows four intramolecular hydrogen bonds of the acidic proton bound to O(2) and the phenolic oxygens O(1), O(4), O(7) and O(10) (Fig. 1a). The residual acidic protons form strong intermolecular hydrogen bonds with solvent (methanol) molecules occluded in the crystal lattice. There are no direct intermolecular hydrogen bonds between neighbouring calixarene acids, in contrast to the frequently observed formation of carboxylic acid dimers.[15]

Compound **1** forms a lamellar structure where the hydrophilic constituents (carboxylic acid residues, crystal methanol solvate) and the hydrophobic residues segregate into different layers. This supramolecular packing arrangement is reminiscent of the bilayer structural motif of membrane forming biogenic lipids and likewise amphiphilic molecules.[16] The bilayers run parallel to the crystallographic *ab*-plane and layer stacking follows the *c*-direction (Fig. 1b). Within the layer, calixarene molecules are close packed with their pseudo C_{4v} symmetry axis being tilted by 24° against the *ab*-plane normal. The average surface area occupied by a single calixarene molecule in the crystal structure of **1** amounts to 1.51 nm^2.

The formation of a planar bilayer is surprising at first, since a close packing of conically shaped amphiphilic molecules should introduce a certain degree of curvature into the interfacial region. However, a calculation of the packing parameter according to Israelachvili *et al.*[17] yields a value close to unity taking the spatial requirements of the methanol molecules into account, which form intermolecular hydrogen bonds with the carboxylic acid headgroups.

Crystal structure of 2. Single crystals of the Ca complex **2** were obtained by slow recrystallization of the crude product from DMSO–H_2O mixtures (5 : 1) held at 98 °C. The X-ray structure analysis once again confirms that the calixarene ligands possess a cone conformation (Fig. 2). The Ca complex may be formally described as a coordination polymer with the sum formula $1/n[Ca(C_{68}H_{92}O_{12}Ca)(H_2O)_2(DMSO)Ca(C_{68}H_{92}O_{12}Ca)(DMSO)_3]_n \cdot 5DMSO$. Apparently, a 1 : 1 complex of a single Ca ion and the octadentate calixarene ligand forms at the beginning, which possesses a two-fold net negative charge under the chosen reaction conditions (excess of $Ca(OH)_2$). The non-coordinated carboxylic acid oxygen donors of each mononuclear $[C_{68}H_{92}O_{12}Ca]^{2-}$ building block can then bind to excess "free" calcium ions in solution to build up a coordination polymer.

The coordination environments of Ca ions in the crystal structure of **2** are quite different: The Ca ions (Ca(1), Ca(2), Fig. 2) sequestered by the calixarene ligand **2** are eight-fold coordinated. The square planes spanned by the phenolic and the carboxylate oxygen donors, respectively, are rotated by 35° against each other. Therefore, the Ca coordination polyhedron may be described as an intermediate form between a square antiprism and a cube. In contrast, the bridging Ca ions (Ca(3), Ca(4)) are in distorted octahedral coordination environments where each Ca ion is coordinated by three monodentate oxygen donors of different calixarene ligands. The coordination environment of Ca(3) is completed by two water ligands and a further oxygen donor of a monodentate DMSO ligand, whereas Ca(4) is further coordinated by three oxygen donors stemming from distinct DMSO ligands.

Due to the stoichiometric (2 : 1) ratio of Ca ions and (deprotonated) calixarene ligands, electrostatically neutral, one-dimensional coordination polymers form which have a dumb-bell shape in cross-sectional view (Fig. 3, left). The coordination strands run in the *b* direction of the crystal lattice. There are no coordinative bonds between coordination strands next to each other, which may explain the high solubility of the complex in non-polar aprotic solvents (*e.g.* trichloromethane). The voids in the packing of coordination strands are filled with (non-coordinated) DMSO molecules. In analogy to the lamellar arrangement of the calixarene moieties in the crystal structure of **1**, compound **2** forms a bilayer structure where the polar functional groups and the hydrophobic residues segregate into different layers. Each bilayer runs parallel to the *ab* crystal plane while distinct bilayers are stacked along the *c* direction (Fig. 3, right). Within the layer, calixarene molecules are close packed with their pseudo C_4 symmetry axis tilted by 24° (34°, respectively) against the *ab*-plane normal. The average surface area occupied by a single calixarene molecule in **2** amounts to 1.70 nm^2.

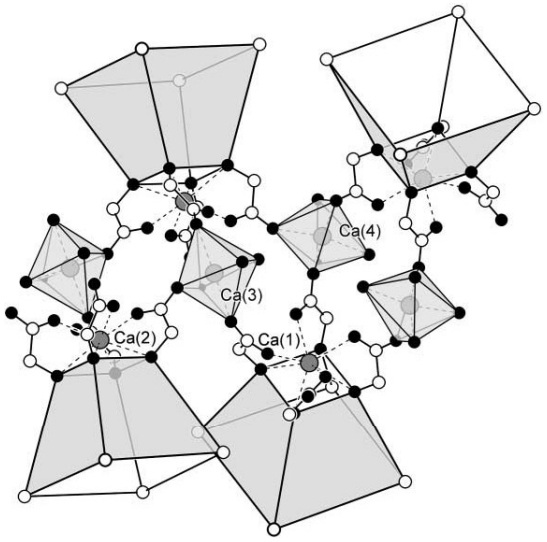

Fig. 2 Simplified representation of the coordination scheme of **2** (coordination polyhedrons are displayed for interconnecting Ca ions only). Selected Ca–O bond lengths and closest Ca ··· Ca non-bonding distances: Ca(1)–O(1) 2.487(2), Ca(1)–O(2) 2.367(2), Ca(1)–O(4) 2.510(2), Ca(1)–O(5) 2.394(3), Ca(1)–O(7) 2.530(2), Ca(1)–O(8) 2.371(2), Ca(1)–O(10) 2.549(2), Ca(1)–O(11) 2.349(2), Ca(2)–O(13) 2.522(2), Ca(2)–O(14) 2.370(2), Ca(2)–O(16) 2.579(2), Ca(2)–O(17) 2.386(2), Ca(2)–O(19) 2.575(2), Ca(2)–O(20) 2.364(2), Ca(2)–O(22) 2.532(2), Ca(2)–O(23) 2.347(2), Ca(3)–O(12) 2.341(2), Ca(3)–O(15) 2.283(2), Ca(3)–O(18) 2.401(2), Ca(3)–O(25) 2.395(3), Ca(3)–O(26) 2.397(3), Ca(3)–O(27) 2.277(3), Ca(4)–O(6) 2.311(3), Ca(4)–O(9) 2.264(3), Ca(4)–O(21) 2.297(3), Ca(4)–O(28) 2.351(3), Ca(4)–O(29) 2.409(6), Ca(4)–O(31) 2.338(6); Ca(1) ··· Ca(3) 6.051(2), Ca(1) ··· Ca(4) 6.511(2), Ca(2) ··· Ca(3) 5.425(2), Ca(2) ··· Ca(4) 6.496(2), Ca(3) ··· Ca(4) 6.542(2) Å.

From the crystal structure analysis important packing parameters can be extracted and compared to the results from Langmuir monolayer investigations.

Monolayer studies

Crystallographic investigations on the solid state structure of the amphiphilic calixarene **1**, and its Ca salt, **2**, were complemented by monolayer studies. An advantage of the monolayer technique using a film balance is that characteristic features of the monolayer, *e.g.* surface pressure, macroscopic texture and lattice structure, can be studied as a function of area per molecule. The surface pressure–area (π–A) isotherms provide information on the thermodynamics and the phase behaviour of the monolayer. Fig. 4 shows the π–A isotherms of compound **1** monolayers spread on aqueous subphases of different compositions (pure water, and 10 mM $CaCl_2$ at different pH values). In all cases, stable monolayers form which collapse upon compression at a surface pressure of ~50 mN m^{-1}. Upon addition of $CaCl_2$, the Langmuir isotherm displays a parallel shift toward higher areas per molecule which is more

Table 1 Area per molecule of (1,1,3,3-tetramethylbutyl)calix[4]arene derivatives as determined from crystal data and Langmuir isotherms

Compound	Area per molecule/nm^2		Inclination angle[a]/°	Ref.
	Crystal structure	Monolayer		
1	1.51	1.45–1.50 (H_2O)	24	This work
2	1.70	1.55–1.60 (10 mM $CaCl_2$)	34, 24[b]	This work
$C_{60}H_{88}O_4 \cdot C_7H_8$	2.25	n.d.	0	11

[a] Angle between the pseudo C_4 symmetry axis of the calixarene molecule and the plane normal of the crystallographic *ab* plane. [b] Two symmetry-independent calixarene molecules per asymmetric unit.

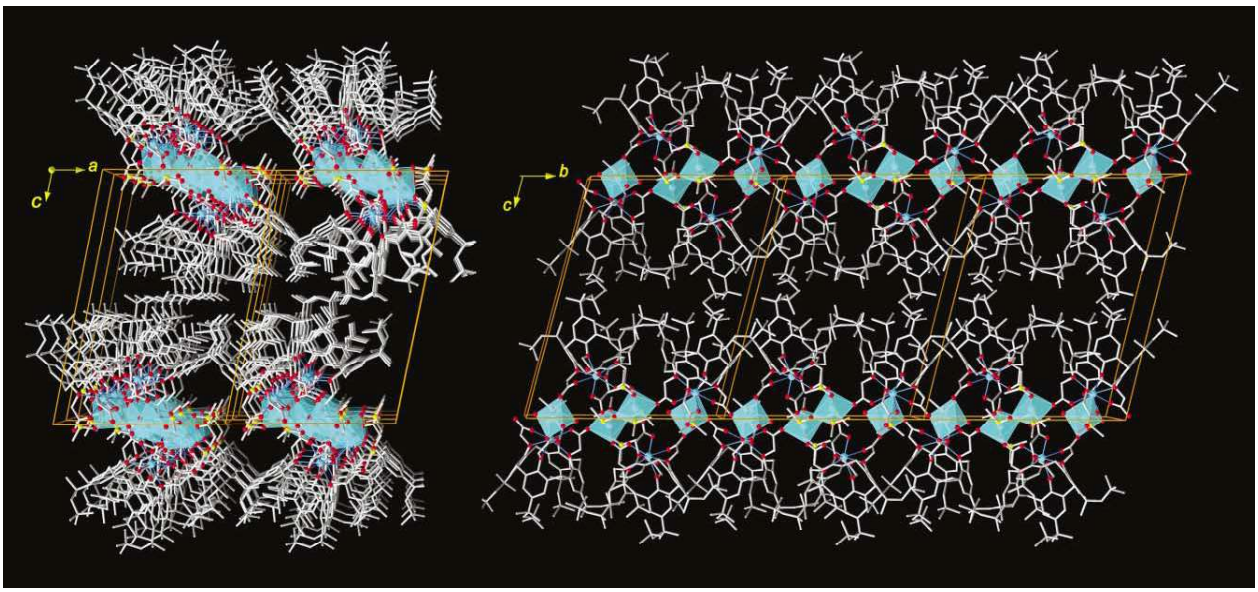

Fig. 3 Wire models of the coordination polymer **2** showing the packing arrangement of the one-dimensional polymeric strands in the crystal lattice. (Solvent DMSO molecules occluded in the crystal lattice and hydrogen atoms are omitted for clarity. Coordination polyhedrons are displayed for interconnecting Ca ions only).

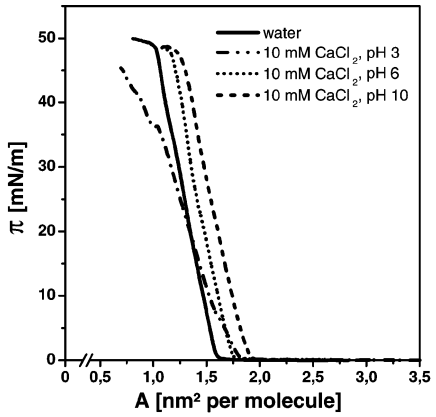

Fig. 4 Surface pressure–area (π–A) isotherms of monolayers of **1** at 24 °C on H_2O, and aqueous 10 mM $CaCl_2$ at different pH values.

pronounced at high pH values. The constant shape of the isotherms indicates a similar phase behaviour for all subphase compositions. The straight pressure increase over a comparatively large region of the molecular area suggests fluid properties for the condensed phase. On a pure aqueous subphase the pressure increase starts at ~1.65 nm^2 molecule^{-1} and on a 10 mM $CaCl_2$ solution at ~1.75 nm^2 molecule^{-1}.

The area per molecule of **1** in the monolayers is estimated from extrapolating the Langmuir isotherms toward zero pressure. The determined area values are listed in Table 1. In both cases, monolayer data are in excellent agreement with the surface area per molecule as determined from crystal structure analysis. On a subphase containing 10 mM $CaCl_2$ at pH 10, the molecular area of **1** shows a significant increase as compared to the corresponding value of the monolayer if spread on pure water. We assume that this behaviour is due to electrostatic/coordinative interactions of Ca ions which cause the carboxylic acid residues of **1** to become deprotonated. Expansion effects of monolayers spread on metal ion-containing subphases, similar to those observed here, have been reported for several systems.[18] The expansion effect is still seen to some extent at pH 3, where deprotonation of the carboxylic acid residues and coordination of Ca ions is expected to be minimal. This observation suggests that formation of a diffuse adsorption layer of Ca ions beneath the monolayer adds to this effect, since adsorption in the interfacial region could lead to a surface pressure rise in accordance with the Gibbs and Langmuir adsorption equation.[19]

The monolayer data show that the packing density of molecules in the monolayer is similar to the density of molecules in the *ab* crystallographic planes of the crystal lattices of **1** and **2**, respectively. However, the featureless compression isotherms point to the fact that the arrangement of molecules in the monolayer is lacking long-range order. The two-dimensional packing of the condensed monolayer phase is obviously determined by the polar head group and not by the alkyl chains (for the latter case, a much more complicated monolayer phase behaviour should be observed). This is in agreement with preliminary results of grazing incidence X-ray diffraction (GIXD) studies which provide information on the packing of the alkyl chains. The measurements revealed that no alkyl chain lattice exists in the condensed monolayer phase.

BAM images of the monolayer of **1** spread on pure water and on a $CaCl_2$ containing aqueous subphase (pH 10), respectively, show that already at zero pressure the fluid-like condensed phase is formed. Both monolayer systems show special features if compared to other amphiphilic monolayers,[20] namely at the beginning, the condensed and gaseous phase are separated by

straight interfaces. A slight compression to a low surface pressure (0.1 mN m^{-1}) causes the condensed phase to grow into the gaseous phase in the form of irregular out-turnings which branch increasingly and transform into foam-like textures (Fig. 5). Upon further compression, a homogeneous condensed

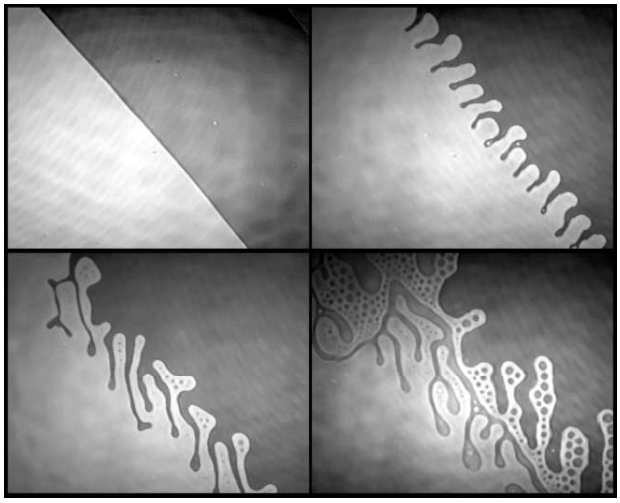

Fig. 5 BAM micrographs of monolayers of **1** at 24 °C on 10 mM $CaCl_2$. Monolayer domains appear as light regions. All micrographs were recorded at identical surface pressure (π = 0.1 mN m^{-1}) within a period of 5 minutes. (Scanned image area: 450 × 400 μm).

phase immediately forms at low surface pressure (>1 mN m^{-1}) which does not show optical anisotropic changes during further pressure increases (BAM image not shown). The phase region which displays the irregular coexistence of the fluid condensed and the gaseous monolayer phase ($\pi \approx$ 0.1 mN m^{-1}) provides optimal conditions for the growth of uniformly oriented calcite single-crystals. The area per molecule at $\pi \approx$ 0.1 mN m^{-1} amounts to 1.70–1.80 nm^2 $molecule^{-1}$ which is in good agreement with the cross-sectional molecular area of compound **2** (1.70 nm^2 $molecule^{-1}$) as calculated from the crystal data.

$CaCO_3$ crystallization underneath monolayers

Crystallization of calcium carbonate underneath monolayers of **1** leads to formation of uniformly oriented calcite single crystals at low compression (π = 0.1–0.5 mN m^{-1}), while more randomly oriented single crystals with comparable nucleation density are obtained at higher surface pressure (π = 5–20 mN m^{-1}).[21] Crystal growth is observed *in situ* by (polarization) optical microscopy (Fig. 6).

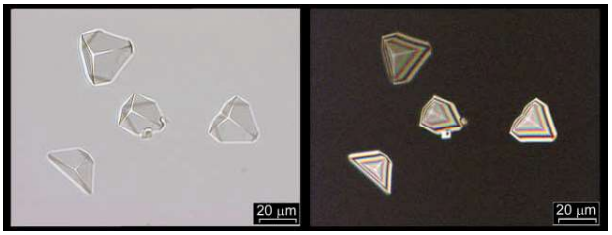

Fig. 6 Left: optical micrograph (brightfield) of (012) oriented calcite single crystals grown under a monolayer of **1** after 3 h. (π = 0.1 mN m^{-1}, $[Ca(HCO_3)_2]_{t=0}$ = 9 mM). Right: Same crystal specimen observed in plane polarized light. (The viewing direction is parallel to the monolayer surface normal, crystals are observed from below the aqueous subphase).

$CaCO_3$ crystals grown under monolayers of **1** show the characteristic shape of a (truncated) calcite {104} cleavage rhombohedron. The simple crystal morphology allows determination of crystal orientation(s) from scanning electron micrographs (optical micrographs, respectively). A projection of rhombohedral faces onto the image plane of the micrograph yields characteristic interfacial angles, which can be assigned to the crystal's orientation. Thus, angle values determined from several micrographs such as those in Figs. 6 or 7 (left) result in

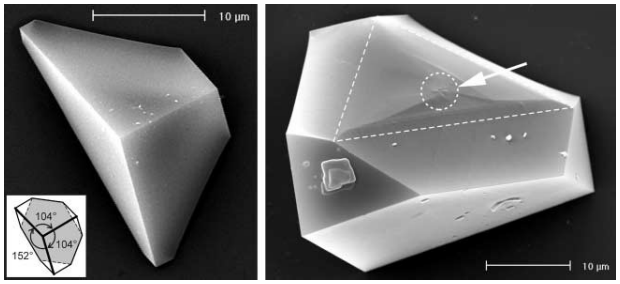

Fig. 7 Left: Scanning electron micrograph (crystals collected after 6 h) of (012) oriented calcite single crystals grown under a monolayer of **1**. (π = 0.1 mN m^{-1}, $[Ca(HCO_3)_2]_{t=0}$ = 9 mM). The inset shows the scheme of characteristic interfacial angles gleaned from the projection of {104} rhombohedral faces of a (012) oriented calcite single crystal onto the image plane of the micrograph. Right: Same crystal specimen observed from the opposite direction. The intercepted line in the micrograph indicates the region of the calcite (012) growth plane which attaches to the monolayer. The white arrow and the circle highlight a central elevated feature in the (012) growth plane, which is common to all crystals that were grown beneath the monolayer.

averages of about 152(±2), 104(±4), and 104(±4)° which are characteristic of (012) oriented calcite rhombohedra.[5c] The (012) plane of calcite single crystals grown underneath monolayers of **1** show distinctive morphological features as presented in Fig. 7 (right side). The white arrow in the electron micrograph indicates the region of the calcite (012) growth plane which attaches to the monolayer during the initial stage of crystal growth. It is seen that the growth plane contains a central elevated feature of irregular morphology (Fig. 7, white circle), which develops into a rough crystal face (Fig. 7, white intercepted line) upon crystal maturation. The fact that the growth plane shows terraces and (microscopic) growth steps which are clearly distinguishable is presumably due to the fact that the crystals become detached from the monolayer due to gravitational forces. Unfortunately, investigations concentrating on the early steps of crystal nucleation, that might help to explain the appearance of the central elevated feature, are less than straightforward. Investigations are underway to examine the morphologically distinguishable regions of the calcite crystal growth planes by means of atomic force microscopy. Clearly, more experimental evidence is needed to characterize the likely mechanisms of crystal nucleation and growth that are operative underneath surfactant monolayers.

Further assignment of the preferential growth direction is gleaned from X-ray powder diffraction (XRPD) measurements in reflection mode on polycrystalline film patches that were transferred onto glass cover slips. Film patches were examined by means of optical microscopy prior to XRPD measurements, in order to ensure that the crystal orientations were preserved during film transfer.

The X-ray powder diffraction pattern of calcite crystals grown underneath monolayers of **1** at π = 0.1 mN m^{-1} is dominated by (012) reflections centered at 2θ = 23.07° (Cu-Kα) of the calcite crystal lattice,[22] while (104) reflections at 2θ = 29.42°, typical of calcite powder samples, are almost completely suppressed (Fig. 8, line (a)). The residual diffraction intensity corresponding to (104) reflections presumably arises from calcite single crystals which have grown spontaneously at the air–water interface. For comparison, crystal growth experiments were repeated under identical experimental conditions but in the absence of a surface monolayer and the resulting film of calcite crystals floating at the air–water interface was transferred onto a glass cover slip. The corresponding diffrac-

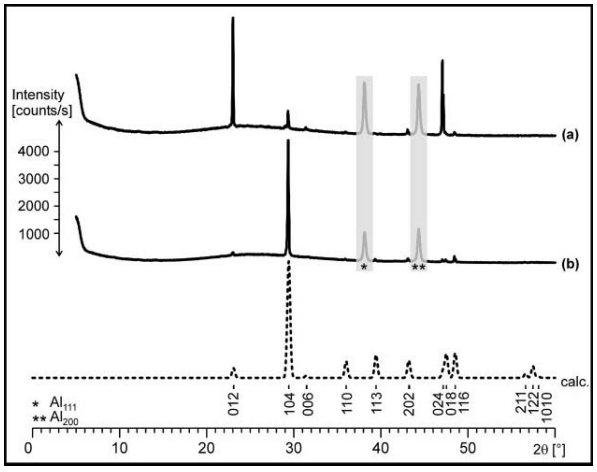

Fig. 8 X-Ray powder diffraction pattern of calcite crystals grown underneath a monolayer of **1** (a, $\pi = 0.1$ mN m^{-1}), and at the air–water interface without monolayer (b). The dashed line represents the calculated diffraction pattern of randomly oriented calcite crystals. (Peaks marked with an asterisk correspond to the (111) and (200) Al reflections of the aluminium supports).

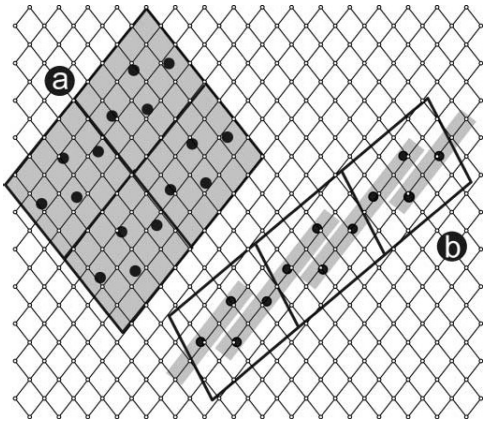

Fig. 9 Schematic representation of geometric correlations between the *ab* plane of the crystal lattice of **2** and the calcite {012} cleavage plane. (a): geometric correlation between the basis vectors of the two different lattice planes; (b): matching of Ca lattice positions at unidirectional lattice rows. (Ca ion positions in the lattice of **2** are represented by black circles while those of the calcite lattice are indicated by smaller white circles).

tion pattern reveals exclusive (104) orientation of calcite single crystals (Fig. 8, line (b)), which is expected for a loose collection of calcite single crystals being deposited onto one of the symmetry equivalent {104} faces during film transfer.

The crystal morphology and the diffraction data unequivocally demonstrate that monolayers of **1** exert a pronounced template effect on the growth of calcite single crystals. The crystals show a uniform (012) orientation with the corresponding {012} crystal faces being juxtaposed to the monolayer. The polar {012} cleavage plane of calcite consists of separate layers of Ca and carbonate ions. Stabilization of this high-energy surface results from surface charge neutralization which most likely arises from coordination of anionic ligands, such as compound **1**, to the terminal (012) layer of Ca ions.

In order to examine a possible geometric correlation between the monolayer of **1** and the calcite {012} cleavage plane, the *ab* lattice plane of Ca complex **2** is considered here as a model of the average packing arrangement of calixarene molecules in the monolayer, since the calculated packing density of calixarene molecules in this particular lattice plane (Fig. 3) equals the experimentally determined density of the monolayer (Table 1). In Fig. 9, the crystallographic positions of interconnectiong Ca ions (Ca(3), Ca(4), Fig. 2) in the crystal structure of **2** are drawn as an overlay of the Ca ion position in the calcite {012} cleavage plane. Apparently, a loose geometric correlation exists between the basis vectors of the two different lattice planes (Fig. 9(a)), while the individual matching of Ca lattice positions further improves if unidirectional lattice rows of **2** are projected onto the calcite lattice (Fig. 9(b)). However, in both cases the exact arrangement of calixarene ligands at the interface is hard to predict, considering the fact that the outward-bound Ca ions of the calcite {012} cleavage plane will become hydrated which should lead to considerable relaxation of their atomic positions. The basis vectors of the calcite {012} cleavage plane span a primitive cell ($a = b = 4.048$ Å, $\gamma = 76.07°$) with an area $A = 15.904$ Å^2. The surface charge density thus amounts to $\sigma = +0.1258$ Å^{-2} which is about an order of magnitude higher than the surface charge density calculated for the *ab* crystallographic plane of **2** ($\sigma = -0.0235$ Å^{-2}).[23] This calculation immediately demonstrates that the interface between the calixarene monolayer and the overgrown calcite {012} cleavage plane must contain additional anionic species in order to balance the total amount of charges between the two juxtaposed surfaces. Taking into account that the density of surface hydroxyl and carbonate groups on calcite crystals increases with pH,[24] we have to consider hydroxide and carbonate ions being coordinated to Ca ions of the calcite {012} cleavage plane. Unfortunately, there are no empirical or theoretical studies currently available that focus on the equilibrium structure of this particular calcite cleavage plane,[25] which could serve as a starting point for the construction of atomically refined interface models.

With the crystallographic information presented here on amphiphilic calixarene **1** and its corresponding Ca salt **2**, respectively, molecular dynamics simulations of surfactant monolayer patches attaching to particular (reconstructed) crystal surfaces should become feasible and efforts in this direction are currently underway.

Matrix-templated growth of calcite single crystals showing a preferential (012) orientation has been reported for other self-assembled systems, including polymeric Langmuir–Schaefer films of 10,12-pentacosadiynoic acid,[4c,26] self-assembled monolayers of carboxylate-terminated alkanethiols supported on Ag[5a]or Au substrates,[27] as well as hydrogen-bonded molecular ribbons consisting of *N*,*N*′-dioctadecyltriazine-2,4,6-triamine and a cyanuric acid derivative.[4e] Much effort has been spent on correlating the periodicity of the calcite {012} cleavage plane with the proposed monolayer structures (although experimental evidence such as crystallographic investigations on principal surfactant packing arrangements and Ca ion coordination motifs were not presented). However, it is hard to believe that the coincident growth of (012) oriented calcite crystals underneath monolayers of structurally dissimilar amphiphiles, including those reported here, can be traced back to strict geometrical or even stereochemical matching of the two juxtaposed surfaces in all cases. Since oriented growth of calcite single crystals under monolayers of **1** preferentially occurs at low surface pressure, where the monolayer displays a liquid-condensed phase, an epitaxial correlation of the monolayer (host) lattice and the overgrown calcite {012} crystal face might in fact be ruled out. It is more likely that non-specific film properties such as average charge density or mean dipole moment of the templating monolayer determine the orientation of crystals.[28] Our recent investigations on oriented crystal growth underneath monolayers of *rccc*-5,11,17,23-tetracarboxy-4,6,10,12,16,18,22,24-octa-*O*-methyl-2,8,14,20-tetra(n-undecyl)resorc[4]arene strongly support this hypothesis: in both cases, the (012) orientation of calcite crystals prevailed.[29] While the complementary molecular structures of the calix[4]arene and resorc[4]arene tetraacids lead to completely different packing arrangements and coordination motifs, the average surface area per molecule in the monolayers and thus the average charge density is of comparable size.

Summary

Amphiphilic calixarene derivatives, such as 5,11,17,23-tetrakis-(1,1,3,3-tetramethylbutyl)-25,26,27,28-tetra(carboxymethoxy)-calix[4]arene, **1**, form stable monolayers which can be employed as supramolecular templates for induced calcite crystallization. The use of easy-to-synthesize calixarenes for this particular area of crystal engineering is reported here for the first time.[30] A range of analytical methods are employed to obtain a clear picture of structural factors that govern the occurrence of uniformly oriented calcite crystals growing underneath monolayers of **1**. Thus, the crystal structures of 5,11,17,23-tetrakis-(1,1,3,3-tetramethylbutyl)-25,26,27,28-tetra(carboxymethoxy)-calix[4]arene, **1**, as well as of its Ca salt, **2**, were solved in order to obtain information on typical supramolecular packing arrangements of the macrocyclic surfactants. The free acid **1** forms a lamellar structure where the hydrophilic headgroups and the hydrophobic alkyl chains segregate into different layers. The corresponding Ca salt **2** comprises a structurally rigid Ca complex of the octadentate calixarene ligand. These structural building blocks are interconnected by Ca ions leading to a sandwich type one-dimensional coordination polymer.

Monolayer compression isotherms indicate that the packing density of amphiphilic calixarenes in the monolayers is almost identical to the corresponding arrangement of molecules in the crystal structures. The featureless Langmuir isotherms, however, point to a liquid-condensed state of **1** throughout the investigated compression range. Brewster angle microscopic observations of the monolayer morphology at low surface pressure reveal a highly viscous consistency, which does not change upon further compression. No indications for the occurrence of a liquid-crystalline phase behavior of **1** were found. Uniform, (012) oriented $CaCO_3$ (calcite) single crystals grow underneath monolayers of **1** at low compression (π = 0.1–0.5 mN m^{-1}), while more randomly oriented single crystals are obtained at higher surface pressure (π = 5–20 mN m^{-1}). Considering the liquid-like state of the monolayer during crystal maturation, an epitaxial correlation between the templating monolayer and the overgrowing calcite crystals is ruled out (although a geometrical match between the putative packing arrangement of calixarene molecules in the monolayer and the arrangement of Ca ions in the calcite {012} cleavage plane can be easily constructed). We, therefore, suggest that non-specific monolayer properties such as average charge density or mean dipole moment are the main determinants for templated calcite growth in the present case.[31]

In summary we have to conclude that the rules which govern the selection of a particular calcite crystal growth plane underneath free-floating surfactant monolayers are not well understood. This (necessarily unsatisfying) statement can be extended to biological systems: Examination of the common crystal orientations in a variety of calcifying organisms reveal that aragonite and calcite single crystals most frequently nucleate from the polar *ab* planes. The arrangement of Ca ions in this plane (the shortest distance between Ca^{2+} ions is 4.99 Å in calcite, and 4.69 Å in aragonite, respectively) is geometrically *not* commensurate with the period of amino acid residues in a protein β-strand (approx. 6.9 Å). Moreover—on pointing more or less perpendicular towards the Ca^{2+} ions in the crystal (001) face—the carboxylate residues of the β-pleated sheet cannot continue the parallel arrangement of planar carbonate anions in the underlying layer(s). The current nucleation model thus does not support the picture of a calcite or aragonite single crystal being nucleated from (001) crystal faces by virtue of stereochemical or geometric matching selection principles.

Future investigations using amphiphilic calix[*n*]arenes of larger ring sizes (*n* = 6, 8) will help to improve our understanding on different mechanisms of induced crystallization underneath structurally non-rigid monolayers. A particularly interesting scientific goal is the quest for the minimum size of an array of pre-organized acidic residues which could still act as a template for heteroepitaxial crystal nucleation. Structurally confined macrocycles such as **1** might be ideal candidates to study this challenging problem as long as the three-dimensional structures of naturally occurring macromolecules fulfilling this task remain to be solved.

Experimental

Synthetic procedures and analytical data for 5,11,17,23-tetrakis(1,1,3,3-tetramethylbutyl)-25,26,27,28-tetra(carboxymethoxy)calix[4]arene, **1**, and its Ca salt **2** are available as ESI.

X-Ray crystallographic data for $C_{68}H_{96}O_{12}\cdot4.75CH_3OH\cdot0.25H_2O$ (1)

Colourless crystals of **1** were obtained by recrystallization from methanol–water mixtures (10 : 1 vol.%). A single crystal of **1** was removed from the mother liquor, mounted in inert oil and transferred to the cold gas stream of a Bruker AXS SMART diffractometer.

Crystal data. $C_{68}H_{96}O_{12}\cdot4.75CH_3OH\cdot0.25H_2O$ (**1**): M = 1262.15, triclinic, a = 12.2924(5), b = 12.8365(5), c = 25.2557(11) Å, α = 97.251(1), β = 93.337(1), γ = 107.202(1)°, U = 3757.2(3) Å^3, T = 183(2) K, space group $P\bar{1}$ (no. 2), Z = 2, μ(Mo-Kα) = 1.9 mm^{-1}, 38412 reflections measured, 16065 unique (R_{int} = 0.0341) which were used in all calculations. The final $wR(F^2)$ was 0.2007 (all data).

CCDC reference number 190054.

X-Ray crystallographic data for $[Ca(C_{68}H_{92}O_{12}Ca)(DMSO)_2(H_2O)]\cdot2.5DMSO$ (2)

Block-shaped colourless crystals of **2** grew slowly from a powder suspension of **2** in DMSO–H_2O (5 : 1 vol.%) mixture held at constant temperature (T = 98 °C, 3 d). A single crystal of **2** was removed from the mother liquor, mounted in inert oil and transferred to the cold gas stream of a Bruker AXS SMART diffractometer.

Crystal data. $[Ca(C_{68}H_{92}O_{12}Ca)(DMSO)_2(H_2O)]\cdot2.5DMSO$ (**2**): M = 1551.17, triclinic, a = 17.0762(5), b = 20.4361(7), c = 25.9349(8) Å, α = 102.671(1), β = 98.326(1), γ = 102.872(1)°, U = 8427.9(5) Å^3, T = 183(2) K, space group $P\bar{1}$ (no. 2), Z = 4, μ(Mo-Kα) = 1.9 mm^{-1}, 56343 reflections measured, 35273 unique (R_{int} = 0.0174) which were used in all calculations. The final $wR(F^2)$ was 0.2306 (all data).

CCDC reference number 190055.

See http://www.rsc.org/suppdata/dt/b2/b206912a/ for crystallographic data in CIF or other electronic format.

Brewster angle microscopy (BAM)

A Brewster angle microscope (BAM-2, NFT, Göttingen) mounted on the Langmuir trough, was used to observe the morphology of the monolayers dependent on the state of the spread calixarene monolayer. Therefore, the surface pressure–area (π–A) isotherms of the monolayers were recorded with a computer-interfaced film balance with a surface area of approximately 300 cm². The surface pressure was measured to within 0.1 mN m^{-1} by the Wilhelmy method using a roughened glass plate. All isotherms were obtained with a compression rate of 1.5 Å² molecule^{-1} min^{-1}. A 0.42 mM solution of the monolayer-forming calixarene in chloroform was spread on the aqueous surface by means of a microsyringe. The monolayer was left to equilibrate for a period of 15 min prior to compression. Brewster angle microscopy (BAM) uses the zero reflectance of the air/water surface for parallel (p) polarised light at the incident Brewster angle. The condensed phase of a monolayer leads to a measurable change in reflectivity, thus allowing visualisation of the monolayer morphology without

affecting the monolayer with probes. Optical anisotropy in the monolayer is detected by introducing an analyser into the reflected beam path. The reflected light was detected by means of a CCD camera and recorded on a videotape. The morphological features of the monolayer were monitored with a spatial resolution of ~3 μm. BAM images were recorded at continuous compression or after compression of the monolayer.

Grazing incidence X-ray diffraction (GIXD)

GIXD experiments were performed using the liquid-surface diffractometer on the undulator beamline BW1 at HASYLAB, DESY, Hamburg, Germany to obtain information on the two-dimensional lattice structure of the spread monolayer. Details of the method have been described elsewhere.[32]

$CaCO_3$ crystal growth experiments

Solutions of calcium bicarbonate were prepared by bubbling carbon dioxide gas through a stirred aqueous (Millipore, resistance 18.2 MΩ cm) solution of $Ca(HCO_3)_2$ (9 mM) for a period of 2 h. Compressed films were formed by spreading trichloromethane solutions of the surfactant in order to generate a liquid- or solid-like film at the air–water interface. Crystals were studied at several times either *in situ* by optical (polarization) microscopy (Olympus IX 70) or on cover slips laid on the film. The cover slips were also mounted on scanning electron microscope (SEM) specimen tubs. A Phillips XL30 ESEM operating at 30 keV was used. The calcite crystals were sputtered with Au prior to examination.

Bulk samples for X-ray powder diffraction (XRPD) were obtained by collecting the crystals on cover slips laid on the film and removed horizontally. A Philips PW 1050/70 X-ray powder diffractometer was employed (2θ scans, Bragg–Brentano para-focussing geometry) using Cu-Kα radiation (λ = 1.54 Å). Crystallographic indices are presented in three-index (*hkl*) notation, based on the hexagonal setting of the calcite unit cell ($R\bar{3}c$, a = 4.96 Å, c = 17.002 Å).

Acknowledgements

D. V. thanks the Minerva foundation for a Minerva fellowship. The research was supported by the Deutsche Forschungsgemeinschaft (DFG Schwerpunktprogramm 1117, "Prinzipien der Biomineralisation"; DFG grant Vo829/2–1). Donation of the starting material *p*-1,1,3,3-tetramethylbutylphenol by CONDEA Chemie GmbH (Marl, Germany) is gratefully acknowledged. The authors would also like to thank Prof. Lia Addadi and Prof. Steve Weiner (The Weizmann Institute of Science, Israel) for fruitful discussions.

References and notes

1 (*a*) H. A. Lowenstam and S. Weiner, *On Biomineralization*, Oxford University Press, Oxford, 1989; (*b*) A. P. Wheeler and C. S. Sikes, in *Biomineralization*, S. Mann, ed., VCH, Weinheim, 1989, pp. 95–131.
2 S. Weiner and L. Addadi, *J. Mater. Chem.*, 1997, **7**, 689–702.
3 S. Weiner and L. Addadi, in *Biomineralization*, S. Mann, ed., VCH, Weinheim, 1989, pp. 133–156.
4 (*a*) S. Mann, B. R. Heywood, S. Rajam and J. D. Birchall, *Nature*, 1988, **334**, 692–695; (*b*) S. Rajam, B. R. Heywood, J. B. A. Walker, S. Mann, R. J. Davey and J. D. Birchall, *J. Chem. Soc., Faraday Trans.*, 1991, **87**, 727–734; (*c*) A. Berman, D. J. Ahn, A. Lio, M. Salmeron, A. Reichert and D. Charych, *Science*, 1995, **269**, 515–518; (*d*) G. Xu, N. Yao, I. A. Aksay and J. T. Groves, *J. Am Chem. Soc.*, 1998, **120**, 11977–11985; (*e*) S. Champ, J. A. Dickinson, P. S. Fallon, B. R. Heywood and M. Mascal, *Angew. Chem., Int. Ed.*, 2000, **39**, 2716–2719; (*f*) P. J. J. A. Buijnsters, J. J. J. M. Donners, S. J. Hill, B. R. Heywood, R. J. M. Nolte, B. Zwanenburg and N. A.J.M. Sommerdijk, *Langmuir*, 2001, **17**, 3623–3628.
5 (*a*) J. Aizenberg, A. J. Black and G. M. Whitesides, *J. Am. Chem. Soc.*, 1999, **121**, 4500–4509; (*b*) J. Köther, G. Nelles, R. Seshadri, M. Schaub, H. J. Butt and W. Tremel, *Chem. Eur. J.*, 1998, **4**, 1834–1842; (*c*) D. D. Archibald, S. B. Qadri and B. P. Gaber, *Langmuir*, 1996, **12**, 538–546.
6 As reviewed in D. Volkmer, *Biomineralization in Encyclopedia of Separation Science*, (M. Cooke, C.F. Poole, eds.), Vol. 2 (Crystallization), Academic Press, 2000, pp. 940–950.
7 P. M. Harrison and P. Arosio, *Biochim. Biophys. Acta*, 1996, **1275**, 161–203.
8 (*a*) M. Arbel-Haddad, M. Lahav and L. Leiserowitz, *J. Phys. Chem. B*, 1998, **102**, 1543; (*b*) J. Majewski, R. Popovitz-Biro, R. Edgar, M. Arbel-Haddad, K. Kjaer, W. Bouwman, J. Als-Nielsen, M. Lahav and L. Leiserowitz, *J. Phys. Chem. B.*, 1997, **101**, 8874.
9 A. Arduini, A. Pochini, S. Reverberi and R. Ungano, *J. Chem. Soc., Chem. Commun.*, 1984, 981–982.
10 A. Arduini, A. Pochini, S. Reverberi and R. Ungaro, *Tetrahedron*, 1986, **42**, 2089–2100.
11 CSD codes: CARJAG, CARJEK, ZUVFOL, and SOVJAO.
12 Early examples of numerous crystallographic investigations on host–guest properties of *tert*-butylcalix[4].arene derivatives include: (*a*) G. D. Andreetti, R. Ungaro and A. Pochini, *J. Chem. Soc., Chem. Commun.*, 1979, 1005–1007; (*b*) C. D. Gutsche, B. Dhawan, K. H. No and R. Muthukrishnan, *J. Am. Chem. Soc.*, 1981, **103**, 3782–3792; (*c*) M. Coruzzi, G. D. Andreetti, V. Bocchi, A. Pochini and R. Ungaro, *J. Chem. Soc., Perkin Trans. 2*, 1982, 1133–1138.
13 CSD codes: CARJAG, CARJEK. G. D. Andreetti, A. Pochini and R. Ungaro, *J. Chem. Soc., Perkin Trans. 2*, 1983, 1773–1779.
14 CSD code: ZUVFOL. J. M. Harrowfield, M. Mocerino, B. J. Peachey, B. W. Skelton and A. H. White, *J. Chem. Soc., Dalton Trans.*, 1996, 1687–1699.
15 G. R. Desiraju, *Angew. Chem., Int. Ed. Engl.*, 1995, **34**, 2311–2327.
16 H. Ti Tien, in *Thin Liquid Films*, I. B. Ivanov, ed., Surfactant Science Series, vol. 29, 1988, pp. 927–1057.
17 J. Israelachvili, D. J. Mitchel and B. W. Ninham, *J. Chem. Soc., Faraday Trans.*, 1976, **72**, 1525–1568.
18 (*a*) V. A. Arsentiev and J. Leja, in *Colloid and Interface Science*, vol. 5, M. Kerker, ed., Academic Press, New York, 1976, pp. 251–270; (*b*) G. T. Barnes, in *Colloid Science*, vol. 2, D. H. Everett, ed., Chemical Society, London, 1975, pp. 173–190.
19 S. J. Cooper, R. B. Sessions and S. D. Lubetkin, *Langmuir*, 1997, **13**, 7165–7172.
20 D. Vollhardt, *Adv. Colloid Interface Sci.*, 1996, **64**, 143–171.
21 Crystallization experiments at even higher surface pressure (π > 20 mN/m) were impossible due to the insufficient long-term stability of the monolayer.
22 Joint Committee on Powder Diffraction Standards – International Center for Diffraction Data, Swarthmore, UK, 1986; File No. 24–27 (Calcite).
23 The calculated σ values represent the surface charge density of a calcite (012) cleavage plane consisting of Ca^{2+} ions, and the surface charge density of a close-packed *ab* layer of $[C_{68}H_{92}O_{12}Ca]^{2-}$ units, respectively.
24 O. S. Pokrovsky, J. A. Mielczarski, O. Barres and J. Schott, *Langmuir*, 2000, **16**, 2677–2688.
25 N. H. de Leeuw and S. C. Parker, *J. Phys. Chem. B*, 1998, **102**, 2914–2922.
26 D. J. Ahn, A. Berman and D. Charych, *J. Phys. Chem.*, 1996, **100**, 12455–12461.
27 A. M. Travaille, J. J. J. M. Donners, J. W. Gerritsen, N. A. J. M. Sommerdijk, R. J. M. Nolte and H. van Kempen, *Adv. Mater.*, 2002, **14**, 492–495.
28 (*a*) M. J. Lochhead, S. R. Letellier and V. Vogel, *J. Phys. Chem. B*, 1997, **101**, 10821–10827; (*b*) S. J. Cooper, R. B. Sessions and S. D. Lubetkin, *J. Am. Chem. Soc.*, 1998, **120**, 2090–2098.
29 D. Volkmer, M. Fricke, C. Agena and J. Mattay, *CrystEngComm*, 2002, **4**, 288–295.
30 Monolayers and Langmuir–Blodgett thin films of amphiphilic calixarenes have been reported: (*a*) M. A. Markowitz, V. Janout, D. G. Castner and S. L. Regen, *J. Am. Chem. Soc.*, 1989, **111**, 8192–8200; (*b*) W. Lee, R. A. Hendel, P. Dedek, V. Janout and S. L. Regen, *J. Am. Chem. Soc.*, 1995, **117**, 6793–6794; (*c*) F. Davis, L. O'Toole, R. Short and C. J. M. Stirling, *Langmuir*, 1996, **12**, 1892–1894; (*d*) A. V. Nabok, T. Richardson, F. Davis and C. J. M. Stirling, *Langmuir*, 1997, **13**, 3198–3201; (*e*) R. A. Hendel, E. Nomura, V. Janout and S. L. Regen, *J. Am. Chem. Soc.*, 1997, **119**, 6909–6918; (*f*) W. He, F. Liu, Z. Ye, Y. Zhang, Z. Guo, L. Zhu, X. Zhai and J. Li, *Langmuir*, 2001, **17**, 1143–1149; (*g*) E. Houel, A. Lazar, E. Da Silva, A. W. Coleman, A. Solovyov, S. Cherenok and V. I. Kalchenko, *Langmuir*, 2002, **18**, 1374–1379.
31 P. Calvert and S. Mann, *Nature*, 1997, **386**, 127–129.
32 V. M. Kaganer, H. Möhwald and P. Dutta, *Rev. Mod. Phys.*, 1999, **71**, 779–820.